International Journal of Modern Physics E
Vol. 24, No. 5 (2015) 1550035 (13 pages)

DOI: 10.1142/S0218301315500354

World Scientific
www.worldscientific.com

Study of elastic and inelastic pion-nucleus scattering using the microscopic model of optical potential

V. K. Lukyanov, E. V. Zemlyanaya and K. V. Lukyanov*
Joint Institute for Nuclear Research,
Dubna 141980, Russia
**lukyanov@theor.jinr.ru*

A. Y. Ellithi and I. A. M. Abdul-Magead
Cairo University, Cairo, Giza, Egypt

Received 23 March 2015
Revised 21 April 2015
Accepted 24 April 2015
Published 14 May 2015

The pion-nucleus microscopic optical potential (OP), defined by the pion-nucleon scattering amplitude and by the generalized density distribution of a target nucleus that incudes internal degrees of freedom, is applied to construct the pion-nucleus differential cross-sections of elastic and inelastic scattering on the nuclei ^{28}Si,^{58}Ni,^{208}Pb at $T_{\rm lab} = 291$ MeV. Calculations are based on the relativistic wave equation and thus relativistic effects and distortions on the relative motion wave functions are taken into account. The respective experimental data are analyzed and the in-medium parameters of the elementary πN-amplitude are established and compared with those from the pion scattering on free nucleons.

Keywords: Pion-nucleus scattering; microscopic optical potential; pion-nucleon scattering amplitude.

PACS Number(s): 25.80.Dj, 24.10.Ht, 21.10.Gv, 21.10.Ft

1. Introduction

The pion-nucleus optical potential (OP) at intermediate energies was first proposed in Ref. 1, and later on it was transformed to the more simple local form in Refs. 2 and 3. Based on this OP the large body of experimental data was fitted in Refs. 4 and 5 at the pion energies from 20 to 291 MeV, and thus the set of parameters inherent to this OP was established. The other approach for scattering of π-mesons on nuclei was developed based on the high-energy approximation (HEA) for scattering theory.[6,7] So, in the early paper,[8] the $\pi^{+16}O$ and $\pi^{-}C^{12}$ elastic scattering data were explained utilizing six parameters for every π^{+} and π^{-} amplitudes of scattering on protons and neutrons, separately. Later on in practice, many applications were made using the joint isospin-averaged 3-parameter πN-amplitude (see, e.g., Ref. 9 and references therein). However, in such approach problems arise to account for

the meson trajectory distortions by the external nuclear and Coulomb potentials when calculating eikonal phases.

Below, to analyze pion-nucleus scattering, we start with the microscopic folding OP $U(r)$ derived in Ref. 10 for elastic scattering. This OP has been successfully applied for elastic scattering of the light exotic nuclei and also of the K- and π-mesons on nuclei (see, e.g., Refs. 11–13). It is based on the nuclear density form factor and the pion-nucleon amplitude of scattering, its form is rather simple and convenient for applications. Moreover, when using this OP at intermediate energies one can avoid problems when accounting for the above mentioned effects of the trajectory distortions on the scattering cross-sections. Instead, for calculations of cross-sections, we apply the Klein–Gordon equation and thus take into account the relativistic and distortion effects exactly. Also, this folding potential can be easily presented in a generalized form by introducing the small axiallity of the distance vector $\mathbf{r}$ of motions. Thus, one can obtain the respective OP $U(\mathbf{r}, \{\alpha_{\lambda\mu}\})$ dependent on the deformation parameters $\alpha_{\lambda\mu}$ inherent to the collective motion of a nucleus. This enables one to estimate the inelastic cross-sections with excitations of the low lying 2^+ and 3^- collective states of nuclei. The object of this paper is the detailed consideration of elastic and inelastic scattering of pions from nuclei at 291 MeV. This energy is expected to be some kind of the boundary energy where effects revealed at lower 33-resonance energies become weak and thus the question arises if it is possible with a help of the free πN scattering amplitude, to get the π-nucleus microscopic OP and thus to explain the π-nucleus elastic and inelastic scattering data without any corrections on the in-medium effects.

In Sec. 2, we present the main formulas for construction of the πA microscopic OP. Calculations of the πA elastic cross-sections are made in Secs. 3 and 4 to understand effects of input parameters of the free and in-medium πN-amplitudes. Section 5 presents calculations of the πA inelastic scattering with excitations of the quadruple 2^+ and octuple 3^- collective states of the same nuclei. Conclusions are done in Sec. 6.

2. Direct and Transition Potentials

The microscopic model of OP developed in Ref. 10 was constructed so that as to reproduce the phase of the high-energy multiple scattering Glauber theory in its so-called optical limit. Below the model elaborated for elastic scattering will be generalized to study inelastic scattering, too. The microscopic OP inherent in pion scattering on spherical nuclei has the form

$$U_{\rm opt}(r) = -\frac{(\hbar c)\beta_c}{(2\pi)^2} \sum_{N=p,n} \sigma_{\pi N}[i + \alpha_{\pi N}] \cdot \int_0^\infty j_0(qr)\rho_N(q) f_{\pi N}(q) q^2 dq, \qquad (1)$$

where $\rho_N(q)$ is the form factor of a density distribution of bare nucleons in a nucleus normalized to Z for protons or to A–Z for neutrons, while $\sigma_{\pi N}$ and $\alpha_{\pi N}$ are total πN cross-section and the ratio of the real to the imaginary part of the pion-nucleon

amplitude of scattering at forward angles

$$F_{\pi N}(q) = \frac{k}{4\pi}\sigma_{\pi N}[i + \alpha_{\pi N}] \cdot f_{\pi N}(q), \quad f_{\pi N} = e^{-\beta_{\pi N} q^2/2}. \tag{2}$$

Here, $\sigma_{\pi N}$, $\alpha_{\pi N}$ and the slope parameter $\beta_{\pi N}$ are done in a number of works with references to the phase analysis of the pion-nucleon scattering data. Relativistic velocity $\beta_c = v_{\text{c.m.}}/c = k_{\text{lab}}/(E_{\text{lab}} + m_\pi^2/M_A)$ in the c.m. pion-nucleus system is expressed through the energy $E_{\text{lab}} = (k_{\text{lab}}^2 + m_\pi^2)^{1/2} = T_{\text{lab}} + m_\pi$ and momentum k_{lab},[a] and where M_A is the mass of a target nucleus.

The OP (1) can be generalized in the form that allows one to get both the spherically symmetric direct part of OP and also the transition potential responsible to inelastic scattering. To this end, one needs to substitute in (1) the relation

$$j_0(qr) = \frac{1}{4\pi}\int d\hat{q}\exp(-i\mathbf{qr}), \tag{3}$$

and to replace the form factor $\rho_N(q)$ by $\rho_N(\mathbf{q}) = \int \exp(i\mathbf{qr})\rho_N(\mathbf{r})\, d^3r$, where the generalized nuclear density $\rho(\mathbf{r})$ is taken in the axially symmetric form

$$\rho_N(\mathbf{r}) = \rho_N(r) + \rho_{N\lambda}(r)\sum_\mu \alpha_{\lambda\mu}Y_{\lambda\mu}(\hat{r}), \quad \rho_{N\lambda}(r) = -r\frac{d\rho_N(r)}{dr}(r/R)^{\lambda-2}. \tag{4}$$

Here, the second term owes its origin to the small axially symmetric admixture to the radius vector[14]

$$\mathbf{r} = r - r(r/R)^{\lambda-2}\sum_\mu \alpha_{\lambda\mu}Y_{\lambda\mu}(\hat{r}), \quad \lambda = 2, 3, \tag{5}$$

where the deformation parameters $\alpha_{\lambda\mu}$ of the r-space stand for collective variables of nuclei. Finally, one can obtain the generalized OP

$$\begin{aligned} U(\mathbf{r}) &= -\frac{(\hbar c)\beta_c}{2(2\pi)^3}\sum_{N=p,n}\sigma_{\pi N}[i + \alpha_{\pi N}] \cdot \int e^{-i\mathbf{qr}}\rho_N(\mathbf{q})f_{\pi N}(q)d^3q \\ &= U_{\text{opt}}(r) + U_\lambda(r)\sum_\mu \alpha_{\lambda\mu}Y_{\lambda\mu}(\hat{r}), \end{aligned} \tag{6}$$

where $U_{\text{opt}}(r)$ is defined by Eq. (1) while the other term is the transition OP with the multipole index $\lambda = 2, 3$. Its radial part reads

$$U_\lambda(r) = -\frac{(\hbar c)\beta_c}{(2\pi)^2}\sum_{N=p,n}\sigma_{\pi N}\,(i + \alpha_{\pi N})\int j_\lambda(qr)\rho_{N\lambda}(q)f_{\pi N}(q)q^2dq, \tag{7}$$

and

$$\rho_N(q) = 4\pi\int j_0(qr)\rho_N(r)r^2dr, \qquad \rho_{N\lambda}(q) = 4\pi\int j_\lambda(qr)\rho_{N\lambda}(r)r^2dr. \tag{8}$$

[a]In Eq. (1), we use the units MeV and fm, and then $\hbar c = 197 \cdot 327\,\text{MeV}\cdot\text{fm}$. In the other cases, the natural system takes place with units $\hbar = c = 1$, and thus E, T, k and m have the same dimension [MeV].

Here, the spherically symmetric $U_{\rm opt}(r)$ provides elastic scattering calculations while the $U_\lambda(r)$ is the transition potential intended for calculations of inelastic scattering cross-sections with excitations of the 2^+ and 3^- collective states of nuclei. In this process, the Coulomb interaction is also entered consisting of two parts $U_c(r)$ and U^c_λ, that correspond to the deformed unified charge density sphere of the radius $R_c = R_{co}[1 + \sum_\mu \alpha_{\lambda\mu} Y_{\lambda\mu}(\hat{R})]$.

In the pion-nucleus scattering at intermediate energies the relativistic effects play an important role and thus should be taken into account. Therefore, we apply the microscopic OP (1) for solution of the relativistic Klein–Gordon–Fock wave equation transformed at $E \gg |U|$ (see, e.g., Ref. 15) to the form

$$(\Delta + k^2)\psi(\mathbf{r}) = 2\mu U_{\rm eff}(r)\psi(\mathbf{r}), \tag{9}$$

where relativistic momentum k in the π+A c.m. system

$$k = \frac{M_A k_{\rm lab}}{\sqrt{(m_\pi + M_A)^2 + 2M_A T_{\rm lab}}} = \frac{M_A\sqrt{T_{\rm lab}(T_{\rm lab} + 2m_\pi)}}{\sqrt{(m_\pi + M_A)^2 + 2M_A T_{\rm lab}}}, \tag{10}$$

and the effective potential consists of nuclear OP and the Coulomb potential of charged sphere with the radius $R_c = r_c A^{1/3}$, where $r_c = 1.3$ fm:

$$U_{\rm eff}(r) = \gamma^{(r)} \cdot [U_{\rm opt}(r) + U_c(r)]\,, \quad \gamma^{(r)} = \frac{\bar{\mu}}{\mu} = \frac{\bar{m}_\pi}{m_\pi} \cdot \frac{m_\pi + M_A}{\bar{m}_\pi + M_A}. \tag{11}$$

Here, the factor $\gamma^{(r)}$ is the ratio of the relativistic reduce mass $\bar{\mu} = \bar{m}_\pi M_A/(\bar{m}_\pi + M_A)$ to nonrelativistic one $\mu = m_\pi M_A/(m_\pi + M_A)$, where $\bar{m}_\pi = \sqrt{k^2 + m_\pi^2} = T_{\rm c.m.} + m_\pi$. Finally, the transformed wave equation (4) is computed using the programm DWUCK4,[16] and thus one obtains differential and total cross-sections of elastic scattering. So, this approach automatically accounts for effects of relativization and also distortions of the relative motion wave functions in the field of a target nucleus.

3. Pion-Nucleus Scattering with Parameters of the Free πN-Amplitude

In the following, we intend to use the microscopic OP (1) to calculate differential cross-sections and then to fit the latter to the respective experimental data. In fact, in this procedure, one should fit 6 parameters in the case of π^+A scattering, namely, 3 for π^+p- and 3 for π^+n-amplitudes, and the other 6 parameters for the π^-A scattering, separately. Such a complex task of fitting so many parameters is rather hard to be realized, and therefore in practice the number of fitted parameters is reduced by using the isospin symmetry relations

$$\sigma_{\pi^\pm n} = \sigma_{\pi^\mp p}, \quad \alpha_{\pi^\pm n} = \alpha_{\pi^\mp p}, \quad \beta_{\pi^\pm n} = \beta_{\pi^\mp p}. \tag{12}$$

Doing so and setting in (1) the same form for the proton and neutron density distributions $\rho_p = \rho_n = (1/2)\rho$ with $\rho(r)$ normalized to the atomic number A, and

considering nuclei with $Z \simeq N$, one obtains the πA microscopic OP as follows:

$$U_{\rm opt}(r) = -\frac{(\hbar c)\beta_c}{(2\pi)^2}\sigma_{\pi N}[i + \alpha_{\pi N}] \cdot \int_0^\infty j_0(qr)\rho(q)f_{\pi N}(q)q^2 dq, \qquad (13)$$

where

$$\sigma_{\pi N} = \frac{1}{2}[\sigma_{\pi^+ p} + \sigma_{\pi^- p}], \quad \alpha_{\pi N} = \frac{1}{2}[\alpha_{\pi^+ p} + \alpha_{\pi^- p}], \quad f(q) = e^{-\beta_{\pi N} q^2/2}. \qquad (14)$$

This potential depends only on three isospin averaged parameters $\sigma_{\pi N}, \alpha_{\pi N}$ and $\beta_{\pi N}$, and they can be established based on the data of phase shift analysis of $\pi^\pm$-mesons scattered on free protons. On the other hand, the in-medium values of them can be obtained by fitting the OP (13) and respective cross-sections to the data on the pion-nucleus elastic scattering.

In Fig. 1, we present our calculations using parameters of the free πN-amplitude compared to the experimental data from Ref. 17 for differential cross-sections for the $\pi^\pm$-mesons scattered on ^{208}Pb at $T_{\rm lab} = 291$ MeV. In Fig. 1(a) the dash-dotted curves are calculated with the whole set of 12 parameters related to the $\pi^\pm$-meson scattering on free nucleons (Table 1, lines 2 and 4). These parameters we obtained

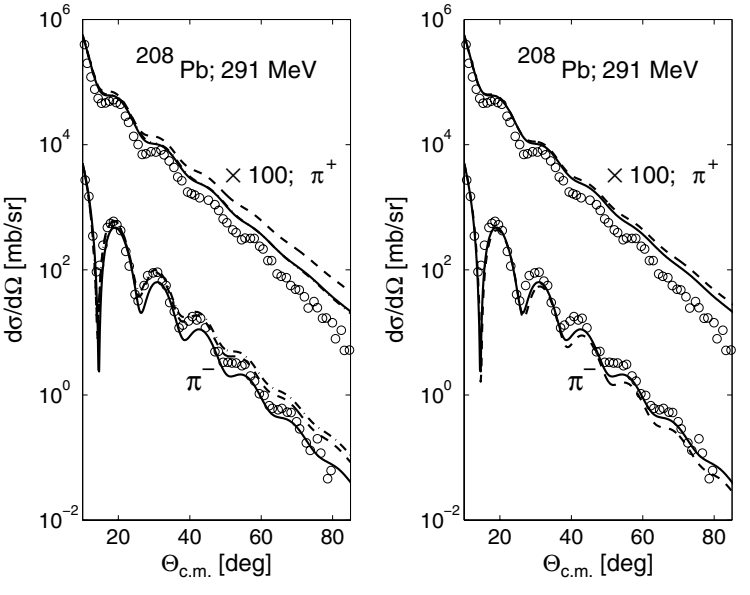

(a) (b)

Fig. 1. Comparison with experimental data[17] of the $\pi^\pm$-meson scattering from ^{208}Pb at $T_{\rm lab} = 291$ MeV. (a) Dash-dotted curves are calculated using 12 parameters extrapolated from free $\pi^\pm n, p$-amplitudes in Ref. 8 (Table 1, lines 2 and 4); solid curves are for the 3 parameters obtained by the isospin averaged 12 parameters used before (see Table 1, line 5); dashes — with 3 averaged parameters extrapolated from those done in Refs. 18 and 19 (Table 1, line 6). (b) Effect of the isospin symmetry violation in scattering of pions from ^{208}Pb; solid curves are for the averaged πN parameters (Table 1, line 6), dashes are when the difference between πp- and πn-cross-sections are taken into account in $\sigma_{\pi N}$ (see the text).

Table 1. Parameters of the free πN-amplitude of scattering at 291 MeV.

σ_{π^-p}, fm^2	α_{π^-p}	β_{π^-p}, fm^2	σ_{π^-n}, fm^2	α_{π^-n}	β_{π^-n}, fm^2	Extrapolation
2.5	−0.45	0.385	6.2	−1.175	0.415	from Ref. 8
σ_{π^+p}, fm^2	α_{π^+p}	β_{π^+p}, fm^2	σ_{π^+n}, fm^2	α_{π^+n}	β_{π^+n}, fm^2	Extrapolation
6.2	−1.175	0.402	2.5	−0.45	0.432	from Ref. 8
$\sigma_{\pi N} = 4.35$, fm^2		$\alpha_{\pi N} = -0.81$		$\beta_{\pi N} = 0.41$, fm^2		Averaged of Ref. 8
$\sigma_{\pi N} = 4.84$, fm^2		$\alpha_{\pi N} = -0.95$		$\beta_{\pi N} = 0.434$, fm^2		Averaged Refs. 18 and 19

by linear extrapolations to the energy 291 MeV of parameters given in Ref. 8 for energies 180, 260 and 270 MeV. Also, based on the obtained set of 12 parameters and using Eqs. (12) and (14), we arrived at the isospin averaged three parameters (Table 1, line 5), and then calculated the OPs Eq. (13) and respective cross-sections, shown by solid curves. The dotted curves correspond to the set of averaged parameters (Table 1, line 6), obtained by extrapolating to the energy 291 MeV of averaged parameters presented in Refs. 18 and 19 at energies $T_{\rm lab}$ from 90 to 280 MeV. It should be mentioned that when calculating OPs, the density distributions $\rho(r)$ of the nuclear protons and neutrons were taken in the form of fermi functions normalized to Z and A–Z with parameters R and a (in fm) to be equal to 3.134 and 0.477 for ^{28}Si;[20] 4.2 and 0.475 for ^{58}Ni;[21] 6.654 and 0.475 for ^{208}Pb.[22] It is seen from Fig. 1(a), that the tested microscopic OPs are working well, and that the usage of free $\pi^{\pm}n$-, $\pi^{\pm}p$-amplitudes and of the πN averaged ones reproduce the general features of an angular distributions of pions scattered on nuclei.

Generally, in the case of scattering from the heavy nucleus ^{208}Pb, the disagreement with experimental data is revealed more obviously than when scattering on the lighter nuclei ^{28}Si and ^{58}Ni. This effect is partly caused by the isospin symmetry violation, and can be estimated if one takes the elementary $\pi^{\pm}$N cross-sections as $\sigma_{\pi^{\pm}N} = ({\rm Z/A})\sigma_{\pi^{\pm}p} + ({\rm N/A})\sigma_{\pi^{\pm}n}$. Substituting there the magnitudes of $\sigma_{\pi^{\pm}p(n)}$ from Table 1, one gets $\sigma_{\pi^+N} = 3.958$ fm^2 and $\sigma_{\pi^-N} = 4.741$ fm^2. The respective pion-nucleus cross-sections are shown in Fig. 1(b) where this effect seems to be too small as compared, say, to disagreements between curves in Fig. 1(a) related to different sets of averaged parameters. So, considering all these effects we would have to conclude that in-medium effect on the πN-amplitude may not be disregarded in the further study of πA elastic scattering.

4. Fit of πA Elastic Scattering and In-Medium πN Parameters

Here, we are aimed to obtain the in-medium averaged parameters $\sigma_{\pi N}, \alpha_{\pi N}$ and $\beta_{\pi N}$ of the πN-amplitude as a result of fitting the calculated cross-sections to the respective experimental data[17] for scattering of π-mesons from nuclei ^{28}Si, ^{58}Ni and ^{208}Pb. Moreover, since the value $\beta_{\pi N}$ is consistent with the πN interaction radius we will not fit it and take $\beta_{\pi N} = 0.434$ fm^2 as done in the free πN scattering. Also, we will not account for the small effect of separate weight contributions of $\sigma_{\pi^{\pm}p}$ and $\sigma_{\pi^{\pm}n}$ into the average $\sigma_{\pi N}$ for nuclei with $Z \neq N$. To estimate numerically the

level of coincidence of such calculations with experimental data, the middle-squared deviations χ^2 were computed using the following expression:

$$\chi^2 = \frac{1}{N}\sum_{i=1}^{N}\frac{\left|d\sigma^{\rm exp}/d\Omega(\theta_i) - d\sigma^{\rm theor}/d\Omega(\theta_i)\right|^2}{\Delta_i^2}, \tag{15}$$

where Δ_i is taken to define the 10% error of the experimental cross-section in a given point number i.

The fitted "in-medium" parameters and corresponding χ^2 magnitudes are presented in Table 2. As an illustration, Fig. 2 shows dynamics of the fitting procedure when the χ^2 deviations come to their minima in three processes $\pi^+ + {}^{28}$Si,^{208}Pb and $\pi^- + {}^{58}$Ni. Comparisons of obtained cross-sections with the whole sets of experimental data are presented in Fig. 3, where solid curves show the fitted cross-sections, and their χ^2 deviations from experimental data one can see in Table 2, line 6. The dashed curves are cross-sections calculated using parameters of the free πN-amplitude, and the respective χ_0^2 for deviations of these curves from experimental data are given in the last line of Table 2. From Table 2, one can get the averaged over three nuclei in-medium πN cross-section $\bar{\sigma} = 4.69$ fm^2, that occurs slightly lower (in about 3%) of the free πN scattering cross-section $\sigma = 4.84$ fm^2. At the same time, the average deflection parameter $\bar{\alpha} = -0.78$ occurs in about 20% larger

Table 2. Parameters of the fitted amplitudes of scattering of pions on the nuclear nucleons.

	^{28}Si		^{58}Ni		^{208}Pb		πN
	π^+	π^-	π^+	π^-	π^+	π^-	free
σ	5.55	4.81	5.43	4.09	4.04	4.23	4.84
α	−0.64	−0.88	−0.68	−1.02	−0.56	−0.92	−0.95
β	0.434		0.434		0.434		0.434
χ^2	2.30	3.56	1.73	4.25	3.94	6.95	
χ_0^2	23.5	5.46	17.7	9.92	676.4	28.1	

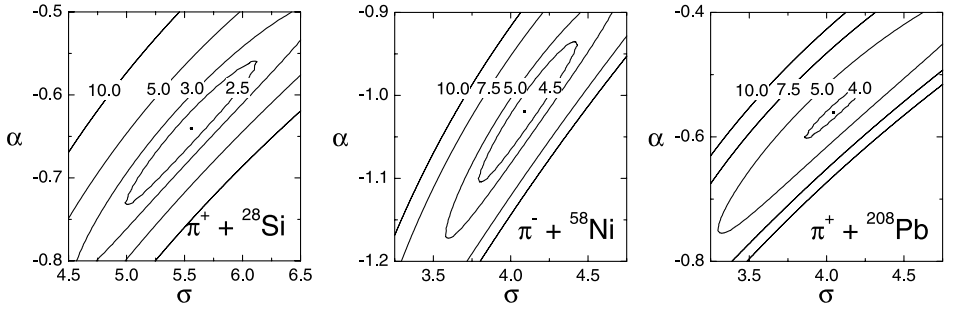

Fig. 2. The numbers on lines in the σ, α planes show the respective χ^2/point values obtained when fitting the calculated to experimental differential cross-sections of the pion scattering on ^{28}Si, ^{58}Ni, ^{208}Pb at $T_{\rm lab} = 291$ MeV.

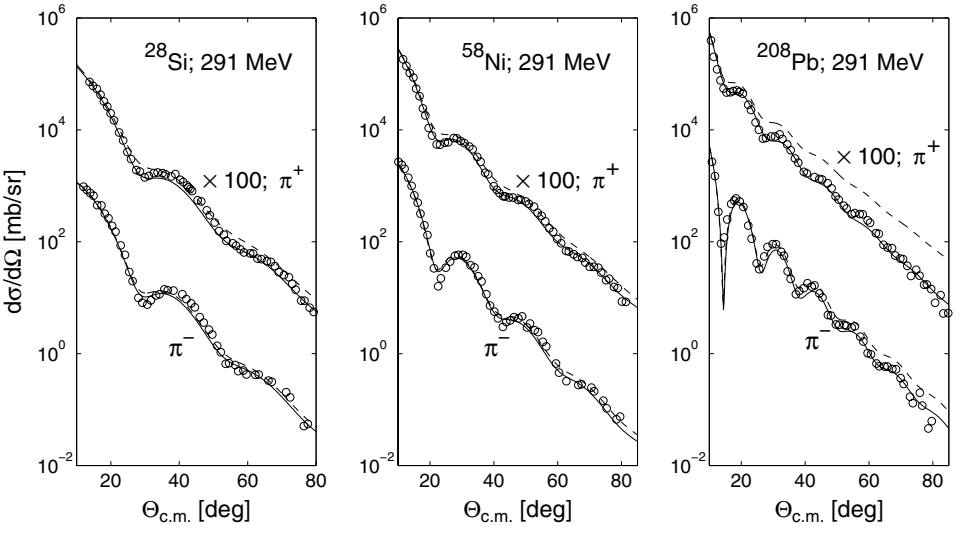

Fig. 3. Comparisons of calculated differential cross-sections of $\pi^{\pm}$-mesons scattered on nuclei ^{28}Si, ^{58}Ni, ^{208}Pb at $T_{\rm lab} = 291$ MeV to experimental data when using the parameters from Table 2. Dashed curves are for parameters of the free πN-amplitude and solid lines are for the fitted parameters.

than the respective free $\alpha = -0.95$. As to the cross-section, one can note that at 291 MeV the πN system takes place at the boundary of exiting of the 33-resonance region where the in-medium effect is determined by two competed factors. One of them is the "swelling" of nucleons in nuclei,[23] that leads to increase of its geometric dimensions and increasing the respective in-medium cross-section, while the other one is the suppression of the interaction of a pion with the bounded nucleon in a nucleus because of the Pauli blocking effect (see, e.g., Refs. 24 and 25). Therefore, in our case when both differential cross-sections are close to each other we can assume that at the energy about 291 MeV the "swelling" and the Pauli blocking effects neutralize each other. With increasing the energy this latter effect becomes weaker, that is seen, for e.g., from the analysis of the pion scattering on the ^{12}C nucleus[26] at comparably larger energy 672 MeV.

5. Inelastic Scattering: Calculations and Comparison with Experimental Data

Based on the transition OPs $U_{\rm inel}(\mathbf{r}, \xi)$ (see Eqs. (6) and (7)) dependent on collective variables responsible for excitations of the quadruple 2^+ and octuple 3^- collective states of nuclei, one can calculate respective pion-nucleus inelastic scattering cross-sections. This scheme does not contain free parameters except the static or dynamic deformation parameters β_λ of nuclei ($\lambda = 2, 3$), that characterize the structure of their rotational or vibrational excited states. As to a transition potential, it includes the nuclear part U_λ depending on a derivative of nuclear density distribution and

also the part U^c_λ that corresponds to the respective $\lambda\mu$ term in an expansion of the Coulomb potential for a unified charge density distribution of the radius $R_c(\alpha_{\lambda\mu})$ as a function of collective coordinates of a nucleus.

The amplitude of inelastic scattering is constructed in the framework of the distorted wave Born approximation (DWBA) where the respective matrix element has a linear dependence on a transition potential while the distorted waves in initial and final channels $\chi^{(\pm)}(\mathbf{r})$ are calculated using the direct $U_{\rm opt}(r)+U_c(r)$ potential, and thus

$$T^{(\lambda)}_{BA}(\mathbf{q}) = \sum_\mu \langle B|\alpha_{\lambda\mu}|A\rangle \int \chi^{(-)*}_b(\mathbf{r},\mathbf{k}_b)[(U_\lambda(r)+U^c_\lambda(r))\,Y_{\lambda\mu}(\hat{r})]\chi^{(+)}_a(\mathbf{r},\mathbf{k}_a)d^3r. \tag{16}$$

Here, the structure matrix element $\langle B|\alpha_{\lambda\mu}|A\rangle$ provides transition from the ground to excited states of even–even nuclei where $|A\rangle = |I_A, M_A\rangle$ $(I_A = M_A = 0)$, $\langle B| = \langle I_B, M_B|$ $(I_A = \lambda, M_A = \mu)$ and thus the matrix element is[14]

$$\begin{aligned}\langle B|\alpha_{\lambda\mu}|A\rangle &= (I_A\,\lambda\,M_A\,\mu|I_B\,M_B)\langle I_B\|\alpha_{\lambda 0}\|I_A\rangle \\ &= (0\,\lambda\,0\,\mu|\lambda\,\mu)\langle\lambda\|\alpha_{\lambda 0}\|0\rangle = (1/\sqrt{2\lambda+1})\beta_\lambda,\end{aligned} \tag{17}$$

where β_λ $(\lambda = 2, 3)$ is a deformation parameter which is fitted in our study.

Numerical calculations of the amplitude (16) are made using the DWUCK4 program[16] where input data include the OP (13) for computing distorted waves $\chi^{(\pm)}$, and the transition potential (7) with the isospin averaged σ, α and β to get differential cross-sections. As to the Coulomb transition potential, it has already been incorporated in the DWUCK4 program in the form inherent in the external part of the unified nuclear charge density distribution to give the result

$$U^c_\lambda(r) = \frac{3Z_AZ_\pi e^2}{2\lambda+1}\cdot\frac{R^\lambda_c}{r^{\lambda+1}}, \quad r > R_c. \tag{18}$$

We calculate cross-sections of inelastic scattering of $\pi^\pm$-mesons on nuclei ^{28}Si, ^{58}Ni and ^{208}Pb at $T_{\rm lab} = 291$ MeV with excitations of the low-lying 2^+ and 3^- collective states, and compare them with experimental data from Ref. 17. In Fig. 4, we show some methodical results useful for understanding the main features of the process. So, Fig. 4(a) exhibits the real and imaginary parts of direct and transition nuclear potentials calculated for the π^+ scattering on ^{208}Pb. One can see that the real parts of both potentials are positive and their areas are approximately equal to each other. Thus, one can expect that the ratio of inelastic to elastic cross-sections will be of the order of $\beta^2_\lambda/(2\lambda+1)$. Indeed, as is seen from Figs. 1 and 4 this ratio at small angles is about 0.02 and thus $\beta_3 \simeq 0.35$, that is only in about 2–3 times larger than customary used magnitudes. Then, Fig. 4(b) demonstrates effect of the Coulomb transition potential on inelastic cross-sections. Here, solid curve is the cross-section calculated when both the nuclear and Coulomb transition potentials $U_\lambda + U^c_\lambda$ are included, and this curve almost coincides with the dotted curve calculated for only nuclear U_λ potential. Such an insignificant effect might be because

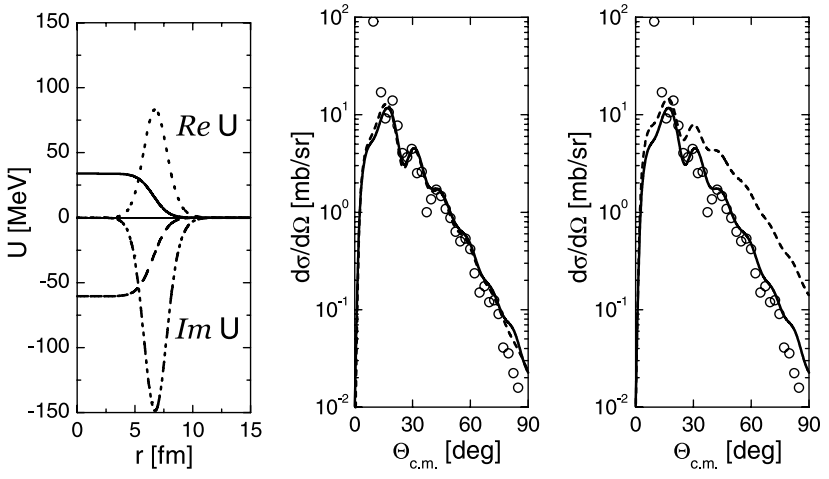

Fig. 4. Inelastic scattering of π^+ mesons on ^{208}Pb at $T_{\rm lab} = 291$ MeV. (a) Upper solid and dotted curves are the real parts of the direct and transition OPs, while the lower dashed and dash-dotted curves are those for the imaginary parts of OPs; (b) Inelastic cross-sections for the 3^- state excitations: Solid — for both Coulomb and nuclear contributions, dotted — for the nuclear excitation only and (c) Calculations for the 3^- excitations: Solid — with in-medium π^+N parameters, dotted — for those of the free π^+N scattering amplitude.

of the destructive interference of a Coulomb and nuclear excitations in the case of π^+ scattering, and also due to the small Coulomb transition potential in a surface region $U^c_{\lambda=3}(R) \simeq 10$ MeV as compared to the nuclear one $U_{\lambda=3}(R) \simeq 75$ MeV as it is done in Fig. 4(a). The other methodical result is shown in Fig. 4(c) where inelastic cross-section calculated with the free πN scattering parameters (dotted curve) occurs in about one order of magnitude larger than the experimental cross-section

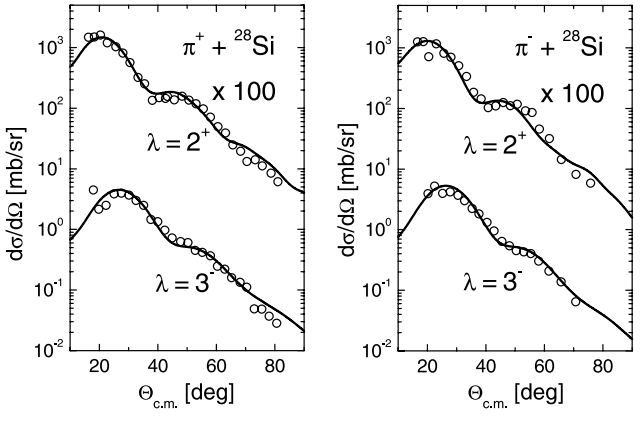

Fig. 5. Comparisons of the calculated inelastic scattering cross-sections for $\pi + {}^{28}$Si at $T_{\rm lab} =$ 291 MeV with experimental data from Ref. 17 (parameters are from Tables 2 and 3).

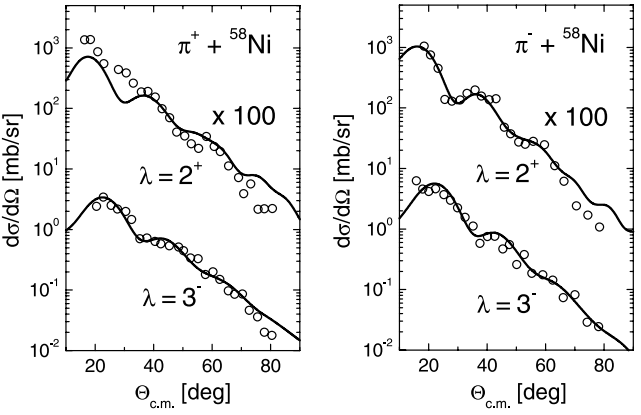

Fig. 6. The same as in Fig. 5 but for the ^{58}Ni.

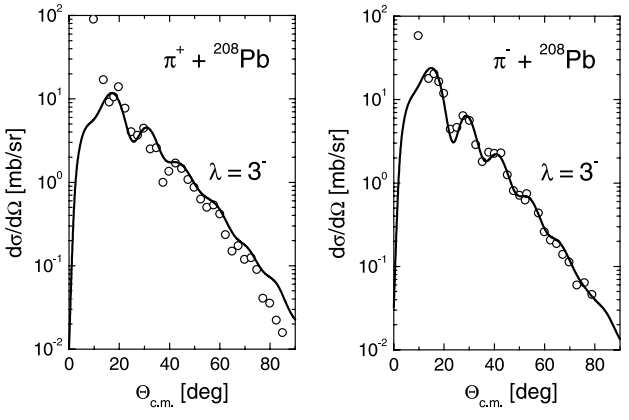

Fig. 7. The same as in Fig. 5 but for the ^{208}Pb.

and the calculated one (solid curve) with the in-medium parameters. The same effect is seen in Fig. 1(a) for elastic scattering too.

Comparisons with the experimental data on the respective inelastic cross-sections from Ref. 17 are shown in Figs. 5–7 where all curves were calculated using the in-medium parameters σ, α and β fitted for the respective elastic cross-sections (solid curves in Fig. 3). It is seen that as a whole our calculations are in a good agreement with experimental data. The deformation parameters β_2, β_3 (see Table 3) were obtained by adjusting the absolute values of cross-sections to the data while the forms of theoretical curves are not distorted in this procedure. In general, the deformation parameters occur in coincidence to each other in about 10% for scattering of π^+- and π^--mesons on the same nuclei. An exception ($\delta\beta_2 \sim$20%) is seen only for the case of scattering on the ^{28}Si nucleus.

Table 3. The deformation parameters and the respective χ^2 deviations obtained from πA inelastic scattering data shown in Figs. 5–7.

The excited state λ		^{28}Si		^{58}Ni		^{208}Pb	
		π^+	π^-	π^+	π^-	π^+	π^-
$\lambda = 2$	β_2	0.48	0.4	0.19	0.19		
	χ^2_2	4.14	11.75	37.24	53.67		
$\lambda = 3$	β_3	0.3	0.3	0.15	0.17	0.14	0.13
	χ^2_3	9.3	3.8	8.54	10.22	21.0	7.8

6. Conclusions

(1) The proposed scheme for studying elastic and inelastic pion-nucleus scattering is based on the microscopic pion-nucleus OP that, in fact, is the folding integral of a nuclear density distribution and the pion-nucleon amplitude of scattering. This scheme differs from that based on a phenomenological OP with the radius assumed to be dependent on the collective variables $\{\alpha_{\lambda\mu}\}$ of a nucleus. Instead, we use the primary characteristic of a nucleus, its density distribution function. Also, an important point is that to calculate cross-sections, we use the relativistic wave equation that makes possible to take exactly into account both the relativistic and distortion effects in initial and final channels of scattering.

(2) Thus when utilizing the microscopic OP we paid attention on the behavior of the elementary pion-nucleon amplitude of scattering and study how the nuclear matter influences on its parameters.

(3) Analyzing the calculated elastic scattering cross-sections of π-mesons on nuclei ^{28}Si,^{58}Ni, ^{208}Pb at 291 MeV, we arrived at the conclusion that the usage of the free $\pi^{\pm}N$-amplitudes does not allow us to get agreement to existing experimental data. This is true for both cases when one applies separate amplitudes of the pion scattering on free protons and neutrons and also for calculations using the joint (isospin averaged) pion-nucleon amplitudes.

(4) Then, we adjusted the theoretical cross-sections to the respective experimental data by fitting the joint parameters of $\pi^{\pm}N$ scattering amplitude and thus obtained its in-medium total cross-section σ and the refraction α parameters, while the shape parameter β_π of πN-interaction was left to be as for the free scattering. As to the in-medium cross-section, its averaged value over three nuclei $\bar{\sigma}$ occurs to be close to the free one, while the averaged refraction parameter $\bar{\alpha}$ turns out to be about 20% difference of the free one, and this result may signify a compensation of some medium factors to each other at this energy region.

(5) As to the inelastic scattering calculations they also can successfully explain experimental data when one uses the same in-medium parameters of the πN-amplitude fitted to elastic scattering data. And the only parameters taken to adjust the absolute values of cross-sections were the quadruple β_2 and octuple β_3 deformations of nuclei.

Acknowledgments

The work was supported by the JINR — Egypt Collaboration Program. E. V. Zemlyanaya, V. K. Lukyanov and K. V. Lukyanov thank RFBR (Grant No. 09-01-00060a) for partial financial support.

References

1. L. S. Kisslinger, *Phys. Rev.* **98** (1955) 761.
2. M. Ericson and T. E. O. Ericson, *Ann. Phys.* **36** (1966) 323.
3. M. Krell and T. E. O. Ericson, *Nucl. Phys. B* **11** (1969) 521.
4. M. B. Johnson and G. R. Satchler, *Ann. Phys. A* **248** (1996) 134.
5. S. A. E. Khallaf and A. A. Ebrahim, *Phys. Rev. C* **62** (2000) 024603; *Phys. Rev. C* **65** (2002) 064605.
6. R. J. Glauber, *Lectures in Theoretical Physics* (Interscience, New York, 1959), p. 315.
7. A. G. Sitenko, *Ukr. Fiz. J.* **4** (1959) 152.
8. H. Lesnyak and L. Lesnyak, *Nucl. Phys. B* **38** (1972) 221.
9. A. S. Shalaby, M. Y. H. Hassan and M. M. H. El-Gogary, *Brazil. J. Phys.* **37** (2007) 388.
10. V. K. Lukyanov, E. V. Zemlyanaya and K. V. Lukyanov, *Phys. A. Nucl.* **69** (2006) 240; *JINR*, preprint P4-2004-115, Dubna, (2004).
11. V. K. Lukyanov, D. N. Kadrev, E. V. Zemlyanaya, A. N. Antonov, K. V. Lukyanov, M. K. Gaidarov and K. Spasova, *Phys. Rev. C* **88** (2013) 034612.
12. V. K. Lukyanov, E. V. Zemlyanaya, K. V. Lukyanov and K. M. Hanna, *Phys. A. Nucl.* **73** (2010) 1443.
13. V. K. Lukyanov, E. V. Zemlyanaya, K. V. Lukyanov, E. I. Zhabitskaya and M. V. Zhabitsky, *Phys. A. Nucl.* **77** (2014) 100.
14. R. G. Satchler, *Direct Nuclear Reactions* (Clarendon Press, Oxford, New York, 1983).
15. R. G. Satchler, *Nucl. Phys. A* **540** (1992) 533.
16. P. D. Kunz and E. Rost, *Computational Nuclear Physics*, eds. K. Langanke *et al.*, Vol. 2 (Springer-Verlag, 1993), p. 88.
17. D. F. Geesaman, C. Olmer, B. Zeidman *et al.*, *Phys. Rev. C* **23** (1981) 2635.
18. M. P. Locher, O. Steinmann and N. Straumann, *Nucl. Phys. B* **27** (1971) 598.
19. A. A. Carter, J. R. Williams, D. V. Bugg *et al.*, *Nucl. Phys. B* **26** (1971) 445.
20. V. K. Lukyanov, E. V. Zemlyanaya and B. Słowinski, *Phys. A. Nucl.* **67** (2004) 1282.
21. M. El-Azab and G. R. Satchler, *Nucl. Phys. A* **438** (1985) 525.
22. J. D. Patterson and R. J. Peterson, *Nucl. Phys. A* **717** (2003) 235.
23. G. E. Brown *et al.*, *Phys. Rev. Lett.* **60** (1988) 2723.
24. E. Oset, H. Toki and W. Weise, *Phys. Rep. C* **83** (1982) 281.
25. C. A. Bertulani and C. De Conti, *Phys. Rev. C* **81** (2010) 064603.
26. M. Mizoguchi and H. Toki, *Nucl. Phys. A* **513** (1990) 685.